Office of Energy Efficiency & Renewable Energy

National Renewable Energy Laboratory

Innovation for Our Energy Future

Modeling and Test-and-Rate Methods for Innovative Thermosiphon Solar Water Heaters

Preprint

J. Burch
National Renewable Energy Laboratory

G. Shoukas, M. Brandemuhl, and M. Krarti
University of Colorado

To be presented at Solar 2006
Denver, Colorado
July 8–13, 2006

Conference Paper
NREL/CP-550-39734
May 2006

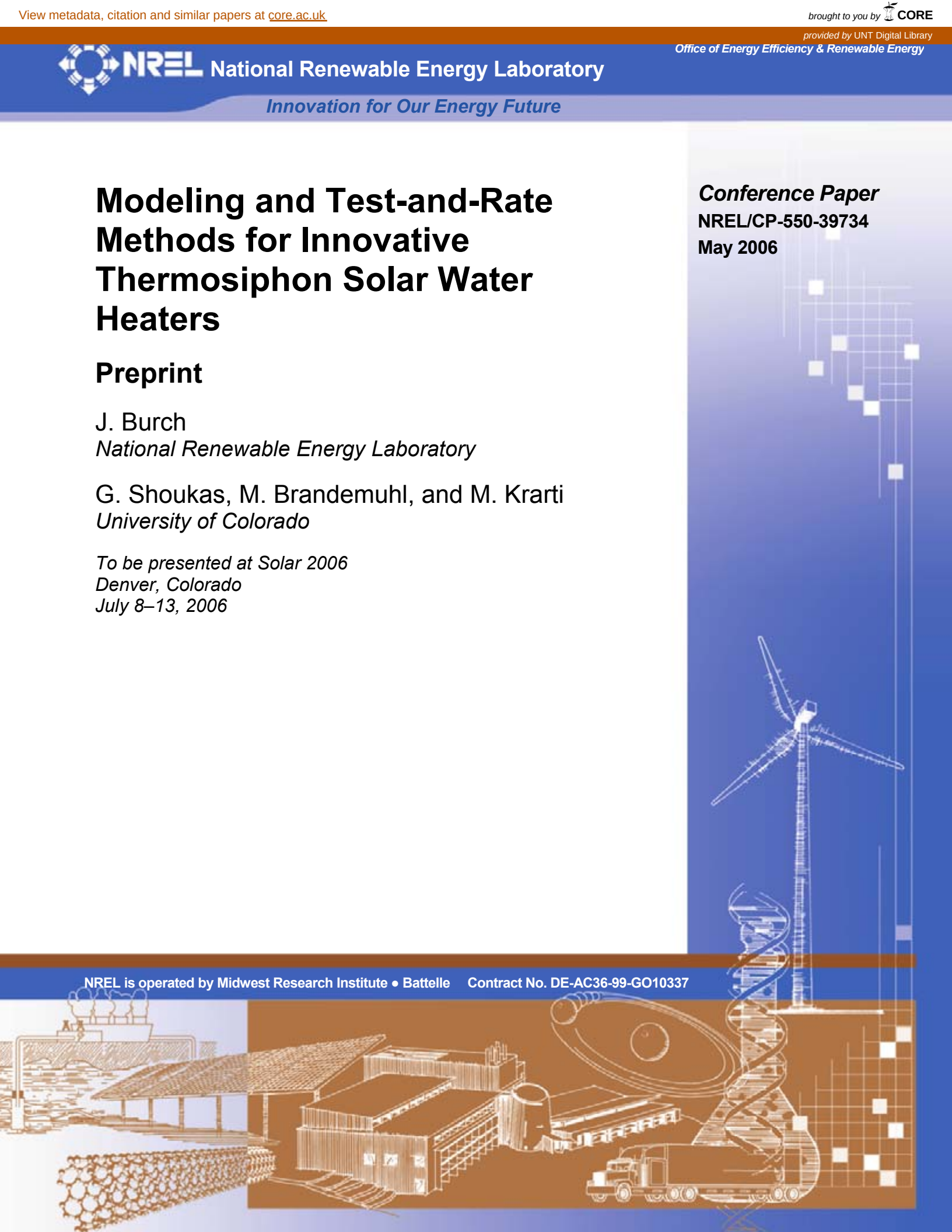

NREL is operated by Midwest Research Institute • Battelle Contract No. DE-AC36-99-GO10337

MODELING AND TEST-AND-RATE METHODS FOR INNOVATIVE THERMOSIPHON SOLAR WATER HEATERS

Jay Burch
National Renewable Energy Laboratory
1617 Cole Blvd.; Golden, CO 80401
E-mail: jay_burch@nrel.gov

Greg Shoukas, Mike Brandemuhl, and Moncef Krarti
University of Colorado at Boulder
Architectural, Civil, and Environmental Engineering
Boulder, CO 80302

ABSTRACT

Simulation models for innovative thermosiphon solar systems (TS) have been generally unavailable, hindering innovative system design/optimization and system rating. A TRNSYS module is introduced that calculates the mass flow rate in general natural convection loops, allows use of any existing tank and heat-exchanger modules, and handles reverse flow in TS when used with a new pipe module. To achieve desired rating accuracy, it is proposed that the flow rate sub-model in the underlying rating simulation be calibrated via nonintrusive flow data from an assembled system. Three innovative TS are being tested to validate the new modeling and the proposed test-and-rate method: two unglazed systems and a glazed polymeric system. An ultrasonic meter and a calorimetric flow-rate method both showed that model friction was high by ~3X. After calibration, the model showed good agreement on both long-term collected energy and tank temperatures.

1. INTRODUCTION

Reducing costs and increasing reliability of solar water heaters (SWH) is believed necessary for a substantial SWH market to exist in the U.S. (1). A strategy for cold climates is expanded use of passive SWH, which include thermosiphon systems (TS), as shown in Fig. 1. TS eliminate the pumps, controller, sensors, and electrical power needed for active systems, and, having insulated storage, perform better than integral-collector-storage during winter in cold climates. However, the market for TS has been limited to warm climates because of the risk of freeze-induced bursting of the supply and return lines (2). Innovative designs for cold-climate TS can be expected if the pipe freeze protection suggested in (3) proves viable. Solving inter-related modeling and rating issues with innovative, low-cost cold-climate TS as in (4) is the goal of this work.

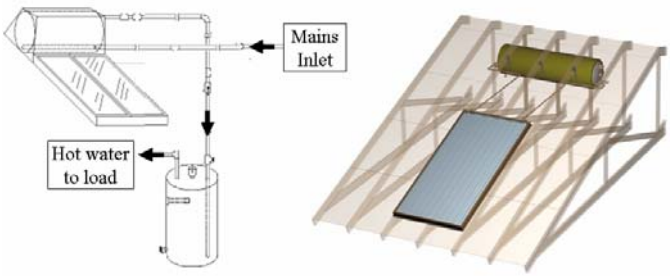

Fig. 1. TS schematic drawings, direct and roof-integrated (5). The simple balance-of-system lowers hardware costs and improves reliability compared to the more common and more complex active systems.

Potential cold-climate TS can be configured in a wide variety of ways. For cold-climate TS, the most obvious collector freeze protection is an indirect glycol loop (although other freeze solutions are possible), with potential variations in the collector-storage heat exchanger including a side-arm counterflow heat exchanger, an immersed coil, a wrap-around coil, and a mantle tank. Various tanks might be used, in vertical or horizontal positions, with a variety of stratification-promoting devices inside the tank. Un-pressurized membrane or thin-walled storage tanks can be lightweight and significantly reduce both hardware and installation costs (4). Potential variations for the heat exchanger between unpressurized tank and pressurized water include immersed coil, tank-in-tank, and side-arm heat exchanger. Unglazed collectors can be used to further lower costs, although performance is reduced by ~30%-50% (4,6). However, there are two inter-related barriers to developing such innovative systems: TS modeling is currently very limited, and there are no established test-and-rate procedures for most potential innovative TS. This work addresses these two issues.

The most common simulation tool for solar thermal design and rating models is the modular and extensible code TRNSYS (7). It is based upon combining "modules" representing components into a system model. However, TS modules in TRNSYS exist for only two TS configurations, direct (Type45) and indirect with pressurized mantle-tanks (8). Neither of these modules calculates reverse flow correctly. For any other natural convection loop (NCL) problem (including TS), it has been necessary to develop new TRNSYS modules, a resource-intensive endeavor. In section 2, a general NCL module is presented that computes the flow rate for any NCL composed of *any* of the components available to TRNSYS, avoiding the development of new modules.

TRNSYS models are also the basis of the Solar Rating and Certification Corporation (SRCC) procedures for rating systems (9). The SRCC system rating procedure is to test key components (collectors, tanks, and heat exchangers) and then to assemble all the components with the measured inputs into a system model that is then used to predict ratings (10). Rating is thus tied to modeling capability; to be practical, models must be easily assembled. Because system performance is not sensitive to flow rate for the high-flow active systems common in the United States, flow rate for these systems has been estimated by the intersection of system friction (with measured $\Delta P_{coll}(m)$) and pump head-flow curves. However, a similar procedure for TS will introduce significantly more error because friction at low flow and in real-world piping systems is hard to estimate accurately. In addition, low flow systems like TS stratify storage, and tank stratification depends ~inversely on flow rate. TS savings are sensitive to tank stratification if there are daytime draws. Section 3 describes tested systems, and Section 4 lays out a process to calibrate the modeled flow rates in TS, with an instantiation of the suggested test-and-rate process in Section 5.

2. GENERAL NCL MODEL

A general NCL schematic is shown in Fig. 2. For TS, the heat source is the collector, the hot leg is collector + return pipe, and the cold leg is the stratified storage tank + supply pipe. The driving force for the flow is the loop buoyancy, which is the difference in weight of the two vertically oriented columns of fluid in the loop:

$$P_{buoy} = \oint \rho \vec{g} \cdot d\vec{s} = (\bar{\rho}_{cold} - \bar{\rho}_{hot})gH \qquad (1)$$

The buoyant pressure is generated by heat sources and sinks exchanging thermal energy with the loop components. P_{buoy} is exactly dissipated by the friction pressure drops around the closed NCL:

$$P_{buoy} = K_{fric} * (P_{fric,shear} + P_{fric,hyd}) \qquad (2)$$

In Eqn. (2), we have separated wall shear and hydraulic fitting losses and we have introduced a friction scale factor (K_{fric}), which will be used to adjust modeled flow to data. Calculations of the pressure drops depend on the component type, as in Table 1. For heat exchangers and collectors, the complexity of flow passages leads one to use only measured pressure drop relationships. Otherwise, correlations of the form $\Delta P(Re;\ldots)$ are used for shear friction.

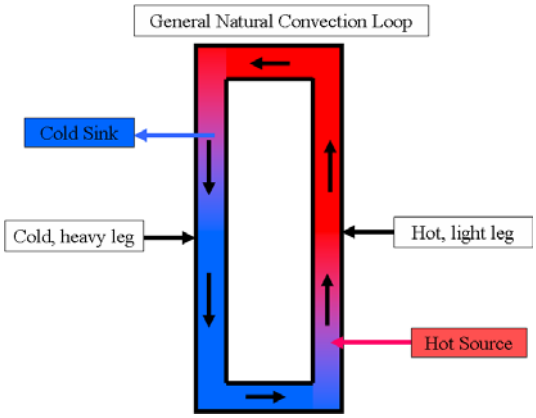

Fig. 2. A general NCL schematic. The fluid rises on the right and descends on the left, with buoyancy maintained by interactions with a heat source (e.g., sun) and/or a heat sink (e.g., heat losses).

For calculation of buoyancy, each component's average temperature is an input to the NCL module. Collector models are based upon collector test data, as in type1 (massless) and type539 (includes mass). Unglazed collectors are modeled as in (6), although necessary modifications have not yet been completed for type539. Heat exchangers could be noded, use the LMTD to generate the average temperature, or use the inlet/outlet average when flows are high and the temperature distribution across the heat exchanger is nearly linear. The TRNSYS pipe module was re-written with a finite difference approach that accounts for pipe mass and allows flow from either direction, enabling consistent calculation of reverse thermosiphoning.

The solution of the coupled equations describing the NCL is based upon the Van Wijngaarden-Dekker-Brent method (11), which shifts optimally between three root-finding methods. Root bounds are estimated as a function of the previous flow. The module computes all pressure drops, including entrance/exit affects between components and pipe friction. The correlations used are shown in Table 1. The solution restarts when flow reversal is indicated. Even with storage above the collector, the model shows consistent reverse thermosiphoning that depends on pipe insulation and is similar to patterns seen in testing. Soluble problems with specified $\Delta P(m)$ relations were used to test the new coding. Module source code and documentation are available on the net (12).

TABLE 1: CALCULATING PRESSURE DROPS

Element in loop	ΔP approach/formula
Components	
Collector or heat exchanger	Measured ΔP(m) input as 2nd order polynomial (from SRCC data)
Pipe	Churchill correlation, with added developing length correlation (12)
Storage tank	Set to zero
Fittings (12)	
Tank expansion	1
Tank contraction	160/Re = 0.5
Pipe expansion	$[1-(d_1/d_2)^2]^2$
Pipe contraction	$0.42[1-(d_1/d_2)^2]^2$
90° elbow	800/Re + 0.25(1 + 1/d)
45° elbow	500/Re + 0.20(1 + 1/d)
Run-thru T	150/Re + 0.50(1 + 1/d)

3. SYSTEM TESTS

To compare unglazed and glazed thermosiphons, and to validate the new modeling and test-and-rate procedure, three TS were put on test (Fig. 3). The area (32 ft^2) and height from collector bottom to tank are the same. The collector loops are direct. The 42-gallon tanks are unpressurized, made of 1/4"-wall polypropylene tanks insulated with 4" of foamboard. Pipe insulation was 1" thick. The two left-most systems (#1, #2) use a polymer pool collector, with the first one glazed with an acrylic sheet. The far right system (#3) uses an unglazed, selectively coated absorber, with emissivity ~0.18 (weathered value, as measured with a Gier-Dunkel DB-100 IR Reflectometer). There was no insulation under or on the sides of the collectors, except for the corrugated back-plane that is part of the recommended installation of system #3. Tank heat can be purged at night through a computer-controlled loop with pump and heat exchanger, which allows control of the tank/system starting temperature the following sunrise.

Tank temperatures are monitored by: a) a thermocouple rake with sensors at the middle of 9 equal-volume tank nodes; and b) a line-averaging RTD extending both top-to-bottom and diagonally across the tank in a sawtooth pattern. Collector inlet-outlet and tank inlet-outlet temperatures are measured. Weather data include ambient temperature, wind speed and direction*, humidity*, solar radiation (global horizontal*, normal beam*, and incidence in the plane) and sky infrared exchange in the plane and on horizontal*. (Note: *'d variables are actually measured at a nearby site (13)). Data are sampled every 5 seconds, and average/totals are stored every 5 minutes.

Figure 3. Three thermosiphon systems on test, with a glazed collector on left and two unglazed collectors to the right.

Measurement of flow rate is challenging because meter flow obstructions change the overall flow. Two non-intrusive techniques were used here, ultrasonic and calorimetric. The ultrasonic meter was available only for two weeks of the testing. The calorimetric method is based on writing the energy balance on the storage tank and solving for the mass flow rate m:

$$m=[C_{tank}dT_{tank}/dt+UA_{tank}(T_{tank}-T_{amb'})]/[c_p(T_{tank,in}-T_{tank,out})] \quad (3)$$

The tank temperature derivative dT_{tank}/dt is calculated by fitting a quadratic curve through 9 points centered on the interval in question, and then taking the derivative of the resulting function evaluated at the midpoint. Tank capacitance C_{tank} includes the tank water, polymeric walls, and immersed instrumentation. $T_{amb'}$ is the area- and conductance-weighted average of T_{amb} and $T_{IR}(\theta)$. UA_{tank} is measured by a night-time temperature decay as in (9), inferring UA_{tank} by the same energy balance approach as in Eq. 3 (but without the mass flow term). Because the tanks are well insulated (~R26), UA_{tank} is sensitive to single-pipe convection and to air-sealing of the pipe penetrations. Table 2 gives results for several combinations of sealing and pipe plugs (which prevent convective flows between tank and pipes). The UA_{tank} value "with seals and plugs" was used in subsequent simulations, considering any additional losses to be accounted for with the piping model.

TABLE 2. UA_{TANK} FOR SEVERAL TANK STATES

Tank State	UA_{tank} [W/°C]
No sealing, and no plugs	1.81
No sealing, with plugs	1.36
With sealing and with plugs	1.04
3-D calculation with manufacturer's k_{foam}	0.56

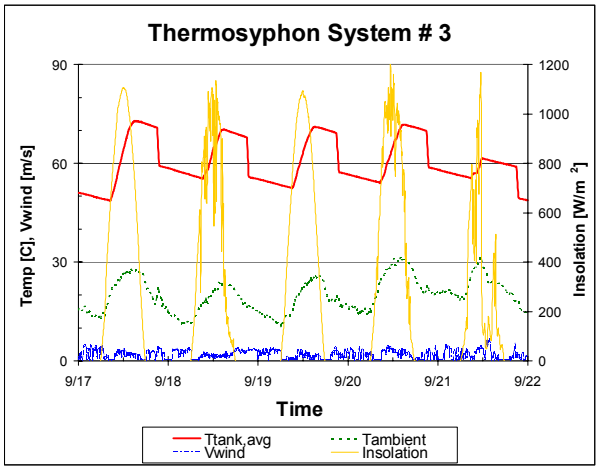

Fig. 4. Weather variables and average tank temperature vs. time for TS #3, with the selective, unglazed collector.

Systems were operated for 45 days in a warm-up mode, with no draws during the day. Data for System #3 is shown in Fig. 4 over a 5-day interval. A heat dump is started at 10 p.m., indicated by the sharp discontinuity in the T_{tank} decay at night. The system starts hot, ~50 °C, during this period. Fig. 5 shows the daily collection efficiency [$Q_{col,day}/(H_{day}*A_{coll})$] versus a daily operating parameter $\Delta T_{avg}/I_{sun,avg}$. As expected, the glazed system operates best, and the selective unglazed system performs better than the non-selective unglazed system. After system models are calibrated for all three systems, annual performance of the systems will be compared for different climates and draw patterns.

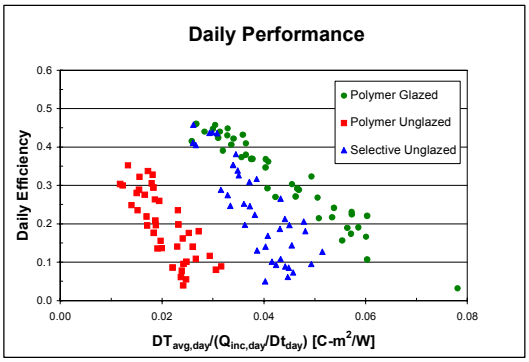

Fig 5. System daily efficiency [$Q_{col,day}/(H_{day}*A_{coll})$] vs. daily operating parameter [$\Delta T_{avg}/I_{sun,avg}$]. Each point corresponds to a warm-up test.

Fig. 6 shows the flow rate as measured by the ultrasonic meter and by tank calorimetry. The flow starts up typically ~1–2 hours after sunrise. The two measurement techniques give roughly the same results on clear days, but the calorimetric technique is comparatively noisy, despite the averaging implicit in obtaining the temperature derivative and rejecting data with low values of ($T_{tank\text{-}in}$-$T_{tank\text{-}out}$). The ultrasonic data shows a characteristic, fairly repeatable pattern after sunset, as seen in Fig. 6. A low flow spike occurs (<~20 l/hr) starting just after sunset, then reverse flow following for several hours, and then a low forward flow (< ~10 l/hr) until sunrise. However, the ultrasonic meter used showed erratic fluctuations of this magnitude when tested in a closed pipe with no flow. Comparison with reverse thermosiphoning predicted by the new TS model has not been completed.

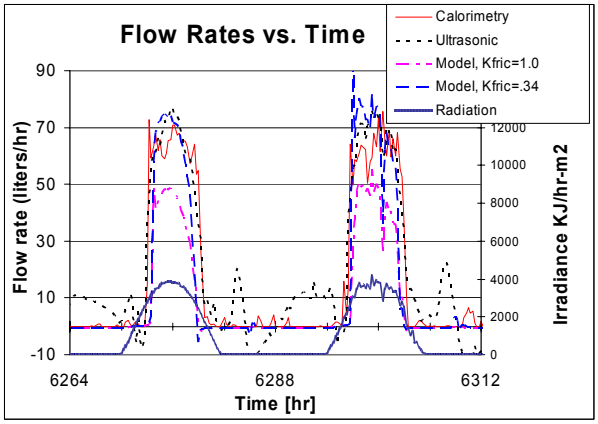

Fig. 6. Flow rate vs. time for system #3, as measured by the ultrasonic meter and the calorimetric method, and as predicted by TRNSYS with K_{fric}=1 and 0.34.

4. MODEL CALIBRATION AND VALIDATION

The key inputs to rating models should be measured, including parameters for collectors, heat exchangers, and storage tanks (10). Certification test results were supplied for the selective collector by the manufacturer (14). For TS models, the collector-loop flow rate is difficult to predict, and this affects tank stratification significantly. The calibration procedure suggested here for TS models is to regress K_{fric} shown in Eqn. 2 through a fit on flow data. The χ^2 metric used for the regression of K_{fric} is:

$$\chi^2(K_{fric}) = \Sigma_i[(m_{model,i}(K_{fric}) - m_{data,i})/\sigma_m]^2/(N_{data}-1), \quad (4)$$

where the dependence of χ^2 and $m_{model,i}$ on K_{fric} is explicitly shown. The regression data were restricted to noon ± 1 hour on days 1, 3 and 4 in Fig. 4 (clear days), avoiding times when noise is relatively high. $\chi^2(K_{fric})$ is displayed in Fig. 7, showing that the model as configured is over-predicting the friction and under-predicting the flow. K_{fric} at χ^2_{min} is somewhat different with the two different mass-flow data sets, 0.44 for the calorimetric method, and ~0.34 for the ultrasonic meter. χ^2 for the ultrasonic data is significantly lower and sharper than for the calorimetric method, reflecting that the ultrasonic data is "less noisy" and on this basis would be preferred to the calorimetric technique. It is also possible to use data on ΔT_{coll} to tune the model flow rate, if accurate testing has been done on the collector.

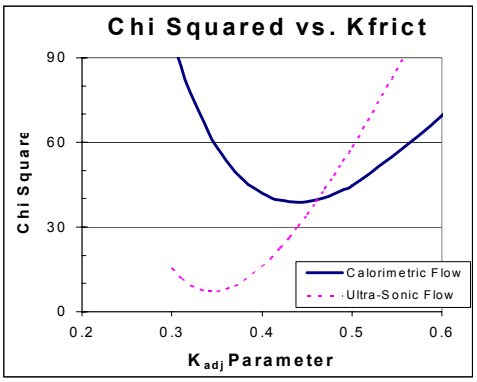

Fig. 7. χ^2 vs. K_{fric}. Two cases were done, with flow rate data from the ultrasonic meter and the calorimetric method.

The calibrated model predictions were compared to 45 days of data on two variables, collected energy [which is proportional to ($T_{tank,sunset}$-$T_{tank,sunrise}$)] and collector temperature rise ΔT_{coll}. This data set has no "real" draws, only a nighttime purge. When validating a ratings model, the data set should include typical draw schedules and a variety of weather. Nonetheless, the data here serves as a reasonable indicator of model accuracy. A comparison on daily temperature rise is shown in Fig. 8. The starting temperature at sunrise heavily influences daily efficiency and temperature rise. Over the entire data set, the average deviation between data and model with K_{fric}=0.34 was 0.4 °C, with a standard deviation of 2.2 °C. The model tends to be low at low wind, and high at high winds, as the wind dependence is not yet present in the unglazed collector model. Fig. 9 shows the relationship between the deviation and wind speed, which indicates some degree of correlation of the error with wind speed (R^2 = .45).

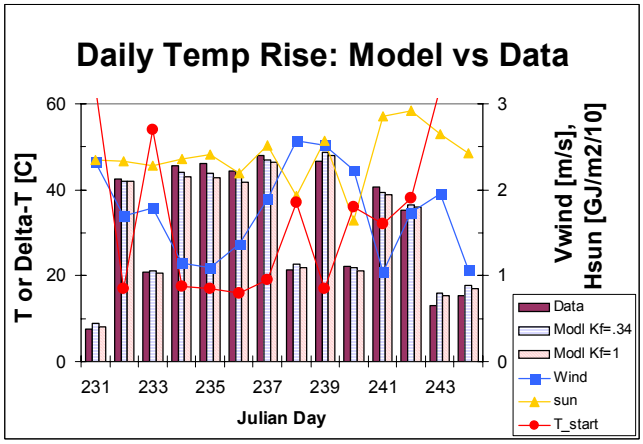

Fig. 8. Comparison between measured and modeled daily temperature rise over a two-week period. Key driving forces are also plotted: wind, sun and warmup starting temperature.

The flow rate calibration significantly impacts predicted ΔT_{coll} and $T_{tank,top}$. $\Delta T_{coll}(t)$ is shown in Fig. 10 for data and for TRNSYS models with K_{fric}=.34, .44, and 1.0. With K_{fric}=1.0, ΔT_{coll} is too high, by about 8 °C midday. ΔT_{coll} is matched the best by K_{fric} = 0.34, and is ~1°C high with K_{fric}=.44. Similarly, $T_{tank,top}$ was too large, and $T_{tank,bottom}$ too cold later in the day, with K_{fric} = 1, consistent with Fig. 10. If there were daytime draws, the temperature rise data would not agree well with the uncalibrated model, because that model would predict incorrect draw temperatures.

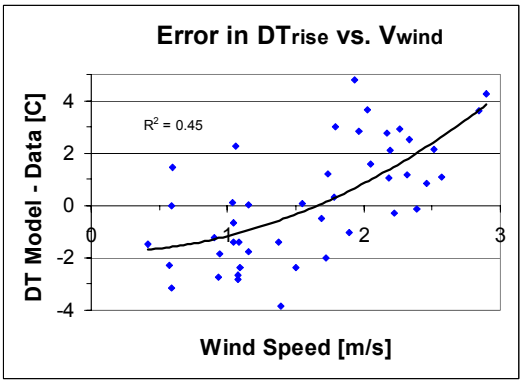

Fig. 9. Relation between error in temperature rise and daytime-average wind speed.

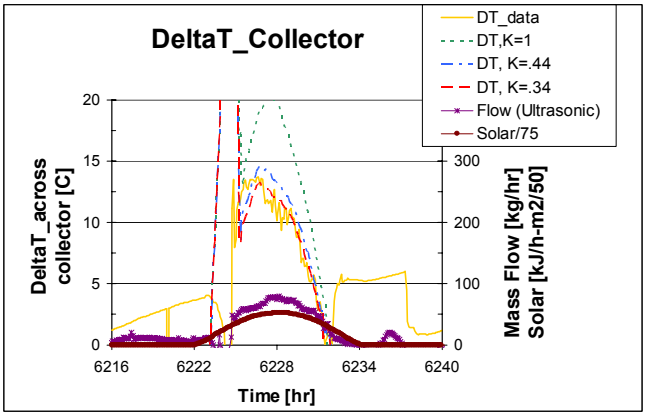

Fig. 10. ΔT_{coll} from data and 3 TRNSYS models vs. time.

6. CONCLUSIONS AND FUTURE WORK

For innovative TS, design optimization and SRCC certification depend on being able to model these systems accurately and easily. To facilitate modeling involving NCL, a general module was developed for TRNSYS that can use any existing component modules and solves the head-friction balance for the loop flow rate. For ratings, the mass flow rate calculations in the model should be adjusted to fit observed data. Three TS systems have been tested, two unglazed (one selective, one non-selective) and one glazed. The model calibration procedure was exemplified on one system. Flows were measured non-intrusively with a calorimetric technique and an ultrasonic flow meter. The

ultrasonic data were less noisy, and led to better agreement with measured $\Delta T_{coll}(t)$ and $T_{tank,top}$. The calibrated model predicted the energy collected over all the warmups to ~1.7%, and closely predicted ΔT_{coll}, $T_{tank,bot}$, and $T_{tank,top}$. The unglazed TRNSYS collector model needs to have wind dependence added, and the test-and-rate method will be validated against normal operation data for all three systems.

7. NOMENCLATURE

Symbols

A	Area
c_p	Heat capacity at constant pressure
C	Capacitance of tank (water + walls)
D	Diameter of air duct
g	Gravity
H	Vertical height of NCL, or Daily solar irradiance
K	Calibration factor for pressure drop calculations
m	mass flow rate
N	Number of data points in the regression
P	Pressure
s	Distance along the path of integration
t	Time
T	Temperature
U	Unit area conductance
ρ	Density (average density with top bar)
χ^2	Metric of deviation between model and data
Δ	Difference
σ	Error
Σ	Summation

Subscripts

amb	Ambient
amb'	Effective temperature (ambient + sky)
bot	Bottom of tank
buoy	Buoyancy
cold	Cold side of the NCL
coll	Collector
data	Data
day	Daytime total or average
fric	Friction
hot	Hot side of the NCL
i	Index for data points
IR	Sky infrared
mod	Model
tank	Thermosiphon system storage tank
top	top of tank

8. ACKNOWLEDGMENTS

The authors acknowledge funding from the U.S. Department of Energy's Solar Energy Technology Program, Solar Heating and Lighting (SH&L) sub-program. We gratefully recognize encouragement from Tex Wilkins and Glen Strahs, SH&L program managers, to pursue low-cost concepts and PSWH market extension.

9. REFERENCES

(1) *Solar Energy Technology Program: Multi-year Technical Plan 2007-2011.* The document is available at http://www1.eere.energy.gov/solar/about.html.

(2) Salasovich, J., Burch, J., and Barker, G., "Pipe Freeze Probability for Passive-solar Water Heating Systems in the United States", *Proc. ASES 2004*. ASES, Boulder, CO.

(3) Burch, J, and Heater, M., "Northward Market Extension for Passive Solar Water Heaters By Using Pipe Freeze Protection with Freeze-tolerant Piping", *Proc. ASES 2006*. ASES, Boulder, CO.

(4) Burch, J., Salasovich, J., and Hillman, T., "Cold-Climate Solar Domestic Water Heating Systems: Life-cycle Analyses and Opportunities for Cost Reduction", *Proc. ASES 2005*. ASES, Boulder, CO., ASES, Boulder, CO.

(5) A thermosiphon schematic from Solargenix, Inc., at: http://www.solargenix.com/hot_water_products.cfm

(6) Burch, J., Salasovich, J., and Hillman, T., "An Assessment of Unglazed Solar Domestic Water Heaters", *Proc. ASES 2005*. ASES, Boulder, CO.

(7) TRNSYS description can be found at: http://sel.me.wisc.edu/trnsys/default.htm

(8) Morrison, G., private communication of the TRNAUS package of thermosiphon and related modules, 3/04.

(9) SRCC. *SRCC Standards OG100, OG300*; and *Test Methods TM-1.* Available at http://solar-rating.org/

(10) Burch, J.; Huggins, J.; Wood, B.; Thornton, J., "Simulation-Based Ratings for Solar Hot Water Systems." *Proc. ASES 1993.* ASES, Boulder, CO.

(11) Press, W., Flannery, B, Teukolsky, S., and Vetterling, W., *Numerical Recipes. The Art of Scientific Computing.* Cambridge University Press, Cambridge, UK. 1989.

(12) NCL module code and documentation are available at: ftp://ftp.nrel.gov/pub/solar_waterheat-out/NCL.

(13) Solar Radiation and Research Laboratory, Golden, CO. National Renewable Energy Laboratory. Data described at http://www.nrel.gov/srrl/ (last accessed 4/06).

(14) Bernard Thiessen, private communication, 4/05. bernard@energie-solaire.com. A test report using DIN EN 12975-2 was provided.

REPORT DOCUMENTATION PAGE

Form Approved
OMB No. 0704-0188

PLEASE DO NOT RETURN YOUR FORM TO THE ABOVE ORGANIZATION.

1. REPORT DATE *(DD-MM-YYYY)*	2. REPORT TYPE	3. DATES COVERED *(From - To)*
May 2006	Conference paper	

4. TITLE AND SUBTITLE
Modeling and Test-and-Rate Methods for Innovative Thermosiphon Solar Water Heaters: Preprint

5a. CONTRACT NUMBER
DE-AC36-99-GO10337

5b. GRANT NUMBER

5c. PROGRAM ELEMENT NUMBER

6. AUTHOR(S)
J. Burch: NREL
G. Shoukas, M. Brandemuhl, and M. Krarti: University of Colorado

5d. PROJECT NUMBER
NREL/CP-550-39734

5e. TASK NUMBER
SH06.2003

5f. WORK UNIT NUMBER

7. PERFORMING ORGANIZATION NAME(S) AND ADDRESS(ES)
National Renewable Energy Laboratory
1617 Cole Blvd.
Golden, CO 80401-3393

8. PERFORMING ORGANIZATION REPORT NUMBER
NREL/CP-550-39734

9. SPONSORING/MONITORING AGENCY NAME(S) AND ADDRESS(ES)

10. SPONSOR/MONITOR'S ACRONYM(S)
NREL

11. SPONSORING/MONITORING AGENCY REPORT NUMBER

12. DISTRIBUTION AVAILABILITY STATEMENT
National Technical Information Service
U.S. Department of Commerce
5285 Port Royal Road
Springfield, VA 22161

13. SUPPLEMENTARY NOTES

14. ABSTRACT *(Maximum 200 Words)*

Simulation models for innovative thermosiphon solar systems (TS) have been generally unavailable, hindering innovative system design/optimization and system rating. A TRNSYS module is introduced that calculates the mass flow rate in general natural convection loops, allows use of any existing tank and heat-exchanger modules, and handles reverse flow in TS when used with a new pipe module. To achieve desired rating accuracy, it is proposed that the flow rate sub-model in the underlying rating simulation be calibrated via nonintrusive flow data from an assembled system. Three innovative TS are being tested to validate the new modeling and the proposed test-and-rate method: two unglazed systems and a glazed polymeric system. An ultrasonic meter and a calorimetric flow-rate method both showed that model friction was high by ~3X. After calibration, the model showed good agreement on both long-term collected energy and tank temperatures.

15. SUBJECT TERMS
solar domestic water heating; solar water heating; cold-climate solar domestic water heating; cold-climate solar water heating; thermosiphon solar water heating; freeze-protection for solar water heating

16. SECURITY CLASSIFICATION OF:			17. LIMITATION OF ABSTRACT	18. NUMBER OF PAGES	19a. NAME OF RESPONSIBLE PERSON
a. REPORT	b. ABSTRACT	c. THIS PAGE			19b. TELEPHONE NUMBER (*Include area code*)
Unclassified	Unclassified	Unclassified	UL		

Standard Form 298 (Rev. 8/98)
Prescribed by ANSI Std. Z39.18